analytical chemistry

Article

pubs.acs.org/ac

Ag Nanoparticles Decorated Cactus-Like Ag Dendrites/Si Nanoneedles as Highly Efficient 3D Surface-Enhanced Raman Scattering Substrates toward Sensitive Sensing

Jian Huang,[†,‡,∥] Dayan Ma,[†,∥] Feng Chen,[‡] Min Bai,[‡] Kewei Xu,[†,§] and Yongxi Zhao*[,‡]

[†]State Key Laboratory for Mechanical Behavior of Materials, School of Materials Science and Engineering, Xi'an Jiaotong University, Xi'an, Shaanxi 710049, P. R. China

[‡]Key Laboratory of Biomedical Information Engineering of Education Ministry, School of Life Science and Technology, Xi'an Jiaotong University, Xi'an, Shaanxi 710049, P. R. China

[§]Xi'an University, Xi'an, Shaanxi 710065, P. R. China

Supporting Information

ABSTRACT: Surface-enhanced Raman scattering (SERS) has been considered as a promising sensing technique to detect low-level analytes. However, its practical application was hindered owing to the lack of uniform SERS substrates for ultrasensitive and reproducible assay. Herein, inspired by the natural cactus structure, we developed a cactus-like 3D nanostructure with uniform and high-density hotspots for highly efficient SERS sensing by both grafting the silicon nanoneedles onto Ag dendrites and subsequent decoration with Ag nanoparticles. The hierarchical scaffolds and high-density hotspots throughout the whole substrate result in great amplification of SERS signal. A high Raman enhancement factor of crystal violet up to 6.6×10^7 was achieved. Using malachite green (MG) as a model target, the fabricated SERS substrates exhibited good reproducibility (RSD ~ 9.3%) and pushed the detection limit down to 10^{-13} M with a wide linear range of 10^{-12} M to 10^{-7} M. Excellent selectivity was also demonstrated by facilely distinguishing MG from its derivative, some organics, and coexistent metal ions. Finally, the practicality and reliability of the 3D SERS substrates were confirmed by the quantitative analysis of spiked MG in environmental water with high recoveries (91.2% to 109.6%). By virtue of the excellent performance (good reproducibility, high sensitivity, and selectivity), the cactus-like 3D SERS substrate has great potential to become a versatile sensing platform in environmental monitoring, food safety, and medical diagnostics.

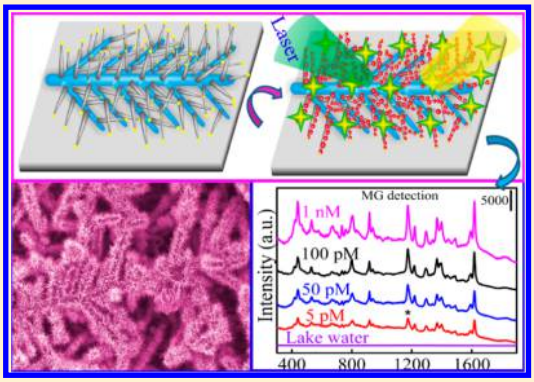

Surface-enhanced Raman scattering (SERS) has been recognized as a promising technique for the efficient sensing of ultratrace analytes since its discovery in the mid-1970s.[1−4] It was widely pursued in various fields due to the rich fingerprinting information on analytes at trace levels or even at single-molecule levels.[5,6] However, the biggest obstacle to the expansion of the scope of practical application for SERS sensing is the lack of highly efficient substrates with uniform and high-density hotspots.[7−9] Recently, extensive efforts have been devoted to construct different SERS substrates from zero-dimensional clusters (Au or Ag nanospheres,[10,11] nanocubes[12,13]) to 3D hierarchical nanoscaffolds (nanoarrays,[14,15] branched nanotrees,[16,17] and nanobutterfly wing[18,19]). Notably, 3D nanostructures are far superior owing to their potential for the arrangement of hotspots along the third dimension. In addition, the hierarchical nanostructures can obtain larger surface area for adsorbing more signal molecules, leading to higher detection sensitivity.

Ag dendrites have been particularly attractive for SERS substrate because their branches have unique electromagnetic field enhancements. Sun and co-workers[20] synthesized the micrometer-scale Ag dendrites in solutions with the enhancement factor (EF) of 5.78×10^3. Li et al.[21] fabricated the Ag dendrites on aluminum foil to obtain enhanced sensing performance (EF was 4.3×10^5). In order to further boost the SERS performance, a promising route is the construction of 3D hierarchical nanostructures. Notably, Ren et al.[22] reported the primitive 3D Ag dendrites with rod-like tips protruding in random directions by the wet-chemical method. Nevertheless, these tips were short and of low density, and the hydrophobic surface challenged the detection of the analytes in water due to the poor affinity.[23−26]

Silicon (Si) nanomaterials have been reported as an excellent SERS platform by He's group because of their biocompatibility, stable chemical structure, hydrophilic properties, and luminescence quenching.[27] The needle-like Si tips rather than nanorods

Received: July 24, 2015
Accepted: September 25, 2015
Published: September 25, 2015

DOI: 10.1021/acs.analchem.5b02788
Anal. Chem. 2015, 87, 10527−10534

Scheme 1. Schematic Illustration of the Fabrication Process of AgNPs Decorated 3D Ag Dendrites/Si Nanoneedles Nanocactus[a]

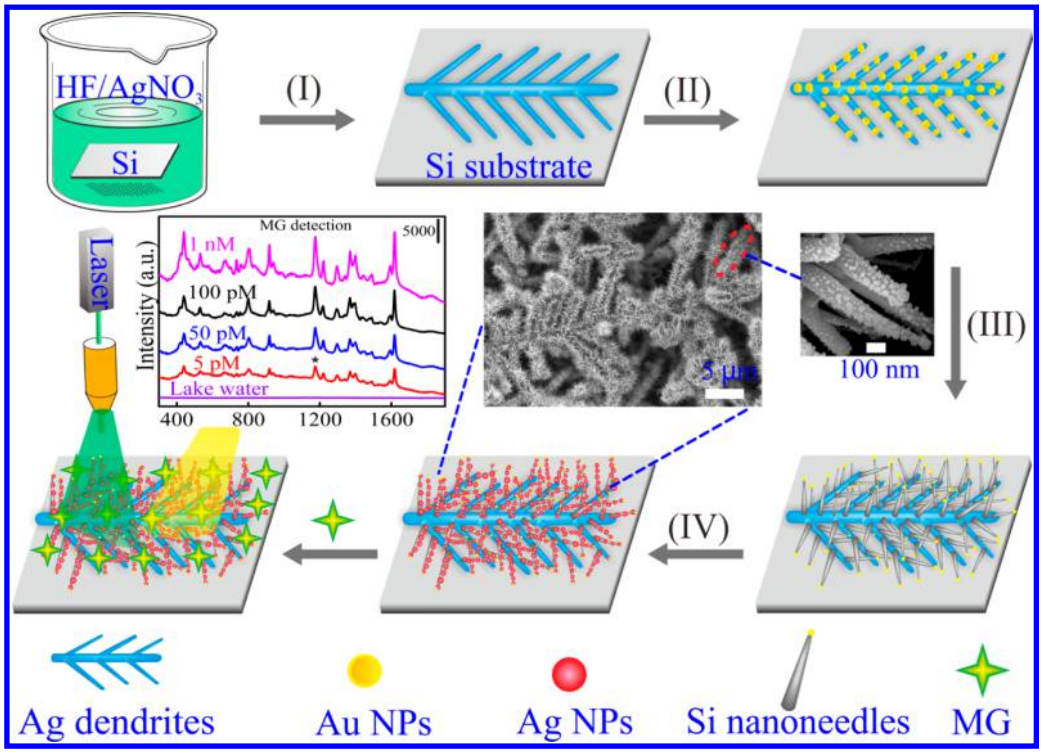

[a](I) Preparation of Ag dendrites; (II) the decoration of AuNPs on the surface of Ag dendrites; (III) the growth of Si nanoneedles; and (IV) nanoneedles were decorated by AgNPs.

or spherical particles were chosen as building blocks to offer additional SERS enhancement by the optical antenna effect.[28] Additionally, grafting the Si nanoneedles onto Ag dendrites also has several other advantages: (1) The Si nanoneedles were used as the scaffolds of Ag nanoparticles (NPs), and they were crucial for chasing high-density hotspots. (2) The hierarchical spatial distribution of Si nanoneedles endowed the Ag dendrites with improved sensitivity and reproducibility. (3) Higher surface area of the 3D nanostructure was responsible for adsorbing more analyte molecules. (4) The hydrophilic nanostructure was very attractive for sensing the analytes in water.

In our previous research, the ZnO nanorods/Si nanoneedles 3D hierarchical nanostructure had been fabricated successfully.[29] However, the preparation of ZnO nanorods arrays suffered from complicated process as well as time-consuming steps and required expensive instruments and very high operating temperature (950 °C). Herein, inspired by these works and the natural cactus composite structure, we developed a unique cactus-like 3D substrate by grafting the Si nanoneedles onto Ag dendrites. The Ag dendrites were exploited as an alternative biocompatible support to overcome the identified deficiencies, in terms of reaction time, growth temperature, and equipment situation. First, it was prepared in beakers at room temperature in a few minutes. Then the Si nanoneedles were grafted onto the Ag dendrites and decorated with AgNPs subsequently. Finally, the prepared SERS substrate was employed for detection of malachite green (MG), a forbidden triphenylmethane dyes in aquaculture that has been reported to cause carcinogenesis, mutagenesis, and chromosomal fractures.[30] The detection limit of MG as low as 10^{-13} M was obtained. Also good reproducibility was demonstrated with low RSD values (<10%) owing to the uniform and high-density hotspots throughout the substrate. Our constructed SERS platform also exhibited excellent selectivity for MG against its derivative as well as coexistent metal ions even in complex mixtures. Furthermore, we demonstrated the practicality and reliability of the 3D SERS substrates via the successful analysis of MG spiked environmental water samples.

EXPERIMENTAL SECTION

Fabrication of Ag Dendrites. Commercial silicon wafer was cut into 2 × 2 cm^2 slices and rinsed with acetone and water for degreasing. Immersion in concentrated 5% hydrofluoric acid was carried out for 30 s to remove the native oxide layer. After rinsing in distilled water and drying in nitrogen atmosphere, the silicon slices were immediately immersed in the mixing of silver nitrate solution (5 mL, 20 mM) and hydrofluoric acid solution (5 mL, 50 mM) for 1 h at room temperature. A large amount of Ag dendrites were formed all over the silicon wafer. Ag dendrites were subsequently rinsed with distilled water twice and then dried in air.

Fabrication of Ag Dendrites/Si Nanoneedles Nanocactus. Si nanoneedles were grafted onto the Ag dendrites by a bottom-up growth process (based on VLS growth mechanism), which was conducted inside plasma enhanced chemical vapor deposition (PECVD) system. The as-prepared Ag dendrites slices were used as the growth substrates, and a mixed silane (10% in hydrogen) was used as the source material for VLS growth. The Ag dendrites slices were coated with a ∼10 nm thick Au layer by ion spurting prior to the PECVD growth. Then, it was placed in a reaction chamber, where the temperature was set at 600 °C. Hydrogen (flow rate, 20 sccm) was used as the carrier gas to transport silane (flow rate,

DOI: 10.1021/acs.analchem.5b02788
Anal. Chem. 2015, 87, 10527−10534

20 sccm) to the reaction zone. The power of radio frequency (rf) was set at 30 W, the deposition pressure was held at 40 Pa, and the deposition duration varied from 15 to 45 min.

AgNPs Decorated Ag Dendrites/Si Nanoneedles Nanocactus. AgNPs were deposited on the Ag dendrites/Si nanoneedles hierarchical structure by a facile galvanic displacement. First, the as-prepared nanocactus were immersed into 5% hydrofluoric acid solution for 2 min (obtain the hydrogen passivation surface). Next, dip the chip into silver nitrate solution for 1 min. The silver ions, which adsorb to the Si nanoneedles, were reduced on the hydrogen passivation surface at the same time. Finally, the samples were carefully washed with double-distilled water and then dried by nitrogen flow for further applications.

RESULTS AND DISCUSSION

Preparation and Characterization of Cactus-Like 3D SERS Substrates. Recently, increasing attention has been paid to the fabrication of 3D hierarchical nanostructures for sensing applications.[31,32] Interestingly, by grafting both Si nanoneedles and AgNPs onto quasi-3D substrate, a cactus-like 3D hierarchical SERS substrate has been developed. Scheme 1 shows the fabrication procedure of such a 3D nanocactus substrate, which comprises SERS-functionalized Ag dendrites (trunk), a large number of hydrophilic Si nanoneedles (branch), and an outer decoration of AgNPs. First, silicon wafer was cut into slices (2×2 cm^2) and immersed into concentrated hydrofluoric acid to remove the native oxide layer. Ag dendrites were prepared by immersing the treated slices in the mixture of silver nitrate and hydrofluoric acid (steps I in Scheme 1) by Feng et al.[33] This process transformed the flat Si wafer into quasi-3D Ag dendrites and defined the length and interval of the branches, and the diameter of the backbones (with a diameter of ~300 nm, a branch interval of 100−200 nm, and the length of 1.6−4 μm). Second, the Si nanoneedles were grafted onto the Ag dendrites through a VLS mechanism in PECVD. The as-prepared Ag dendrites were coated with Au seed before being placed inside the reaction chamber (steps II). As the temperature rises (~600 °C), the catalytic droplets formed on the surface of Ag dendrites. A dilute mixture of silane in hydrogen was initiated with a radio frequency power, which results in the pyrolysis of the silane and the initiation of SiH_x cluster growth (steps III). The SiH_x precipitated at the liquid−substrate interface, and the nanoneedles grew in a layer-by-layer process.

In our experimental conditions, the size of Au droplet gets smaller and smaller owing to the loss and shrinkage, which leads to gradual tapering nanoneedles taking place (A detailed growth mechanism was shown in Scheme S1, Supporting Information). Prior studies have also shown that tapered Si nanowires were synthesized in an ultrahigh vacuum CVD system because of the shrinking seed.[34] After the Si branches were grafted onto the trunk, dense monolayers of AgNPs were attached onto their surfaces by galvanic displacement (step IV, the Si nanoneedles act as reducing agent for the reduction of silver ions). Although Ag dendrites can be used as the SERS substrates directly, the 3D AgNPs decorated Ag dendrites/Si nanoneedles substrates were fabricated here for achieving a much stronger enhancement. It is advantageous for the ordered arrangement of the high-density hotspots along the third dimension direction. Meanwhile, the hierarchical scaffolds and the hydrophilic performance can endow the substrates with improved sensitivity and reproducibility.

Scanning electron microscope (SEM) images show the evolution from Ag dendrites to 3D AgNPs decorated Ag dendrites/Si nanoneedles substrates. The initial Ag dendrites (Figure 1a1−a3) were smooth and lain on the substrate with

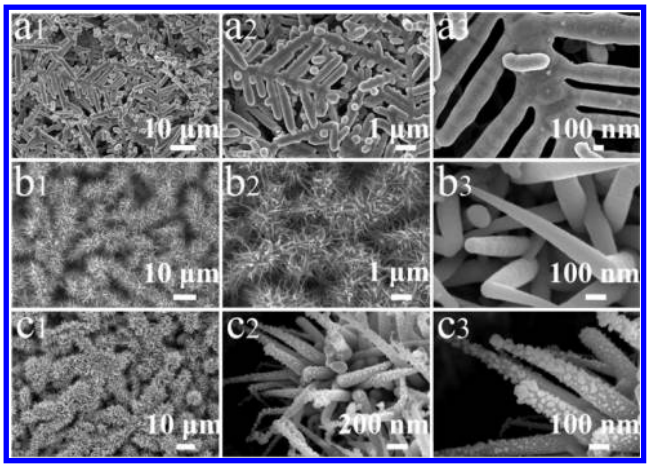

Figure 1. SEM images of the (a1−a3) Ag dendrites, (b1−b3) Ag dendrites/Si nanoneedles nanocactus, and (c1−c3) AgNPs decorated Ag dendrites/Si nanoneedles SERS substrates, at different magnifications.

excellent uniformity that was consistent with most of the previous reports.[35] Once the graft achieved by PECVD, the original smooth dendrites branched out to form 3D cactus-like nanostructure. The typical images of as-prepared Ag dendrites/Si nanoneedles nanocacti are shown in Figure 1b1−b3 at different magnifications. The silicon nanoneedles show cone-like morphology with a typical branch length from 600 nm to 1.2 μm. The bottom diameter of Si nanoneedle is about 150 nm and gradually decreases from the root to the tip which attributes to the loss and shrinkage of the alloy droplet. It is quite clear that this step generates a large number of homogeneous cactus spines (Si nanoneedles), which are employed to improve the wettability and enhance the loading capacity of Ag dendrites scaffolds significantly.

By changing the experimental conditions (such as deposition duration), the size of the branches could be tuned accordingly. As shown in Figure S1, the length of the Si nanoneedles changed from 200 nm to 1.2 μm, and the elements distributions of the trunks and branches were carried out by energy dispersive spectrometer (EDS) in Figure S2 (see Supporting Information). An adjustable size of the branches offers a new opportunity to improve the wettability and SERS properties (owing to its high surface area, hydrophilic performance, and considerable loading capacity). In Figure 1, panels c1−c3 show the representative SEM images of Ag dendrites/Si nanoneedles nanocactus decorated with AgNPs at different magnifications. The average size of AgNPs was approximately 27.0 ± 8.3 nm via the rough statistics. Once AgNPs were immobilized on the Si nanoneedles, a highly efficient SERS substrate formed for sensing detection. To our surprise, the wettability and water contact angle (WCA) differs from the original Ag dendrites (the WCA of Ag dendrites is 129.0°). Our results clearly indicate that the WCA first decreases sharply from 129.0° to 11.4° along with the grafting of Si nanoneedles. When AgNPs were decorated on the surface of Si nanoneedles, it only increases from 11.4° to 14.0°. (A detailed process is shown in Figure S3, Supporting Information.)

DOI: 10.1021/acs.analchem.5b02788
Anal. Chem. 2015, 87, 10527−10534

Additionally, the size, density, and gap of AgNPs were optimized by changing the concentrations of $AgNO_3$, and their SERS properties were shown in Figures S4 and S5. To ensure the assembly quality and obtain relevant structural characteristics, each step of substrate assembly was tracked by X-ray diffraction (XRD), X-ray photoelectron spectroscopy (XPS), and energy dispersive spectrometer (EDS) (Figures S6 and S7, Supporting Information).

Evaluating Sensitivity and Raman Enhancement of 3D SERS Substrates. SERS has been proved as an ultrasensitive method for rapid and label-free detection of illegal ingredient in different fields. Here, the 633 nm laser is chosen for SERS evaluation (Figure S6f, Supporting Information). A widely used SERS probe, CV, was employed to preliminarily evaluate the sensitivity of SERS substrates. First, the lengths of Si nanoneedles, the sizes of AgNPs, the gaps between the neighboring AgNPs, and the hydrophilic performance were effectively adjusted for generating the highest SERS signal intensity. Then, the SERS spectra of CV with different concentrations (from 10^{-6} M to 10^{-12} M) adsorbed on the optimal SERS substrates were measured. As shown in Figure S8a (Supporting Information), the characteristic bands of CV can be identified clearly even at a concentration as low as 10^{-12} M, demonstrating the high sensitivity of SERS substrates. The assignments of all characteristic peaks are listed in Table S1 (Supporting Information). The SERS capability of the as-prepared substrates were evaluated by the EF.[36] A volume of 10 μL of CV aqueous solution with a certain concentration (10^{-9} M) was directly dropped on the as-prepared SERS substrate with an area of 9 mm^2(Figure S8b,curve ii, Supporting Information). Considering an area ratio of approximately 1.1×10^7 between the deposition area and the laser spot ($9\ mm^2/\pi \times 0.25\ \mu m^2$), there was $\sim 6.0 \times 10^9$ molecules ($10\ \mu L \times 10^{-9}$ M $\times 6.02 \times 10^{23}$) within the scope of the laser spot ($\sim 1\ \mu$m in diameter) (assuming uniform distributions of the adsorbed molecules). Besides, the normal Raman spectrum of 0.01 M CV aqueous solution dried on Si wafer was used as the reference (Figure S8b, curve (i)). The SERS EF was estimated to be 6.6×10^7, indicating an excellent enhancement of our SERS platform. It was based on the intensity ratio of typical scattering band at approximately 1179 cm^{-1} from SERS and normal Raman spectra of CV (details were given in the Supporting Information).

Rapid and Ultrasensitive Detection of MG. In recent years, emerging harmful substances and unapproved drug residues in food or drinking water have attracted people's great attention.[37,38] Triphenylmethane dyes, malachite green (MG) has been widely used as effective antifungal and antiparasitic agents in aquaculture since the 1930s. Because of its carcinogenesis, mutagenesis, and toxic effects, it was banned for use in aquaculture operations in many countries.[39] Nevertheless, to be driven by the economic benefits, it probably was illegally used in some small aquaculture farm and discharged into environmental water.[40] Development of a rapid, simple, and sensitive method for detection of these hazardous substances are highly desirable. Currently, several principal strategies have been demonstrated in laboratories, including high-performance liquid chromatography (HPLC),[41] mass spectroscopy (MS),[42] colorimetric detection,[43] electrochemical analyses,[44] and enzyme-linked immunosorbent assay (ELISA), etc.[45,46] However, most of the above approaches are restricted in real life because of the time-consuming steps, complicated sample preparation, as well as requiring expensive instruments and well-trained operators, etc. Therefore, it is of great significance to develop reliable sensing method in terms of sensitivity, reproducibility, assay time, and on-site applicability.

SERS sensing has been focused in different kinds of domains due to their ultrasensitivity and fingerlike structural information. Taking the advantages of the high-density hotspots and the hydrophilic performance of the 3D hierarchical nanostructures, MG molecules can be detected sensitively by SERS sensors. Here, the stock solutions of MG were prepared and diluted in a range of 10^{-6} M to 10^{-13} M. The substrates were immersed into the MG aqueous solution for 20 min before SERS measurement. Figure 2a shows the SERS spectra of MG

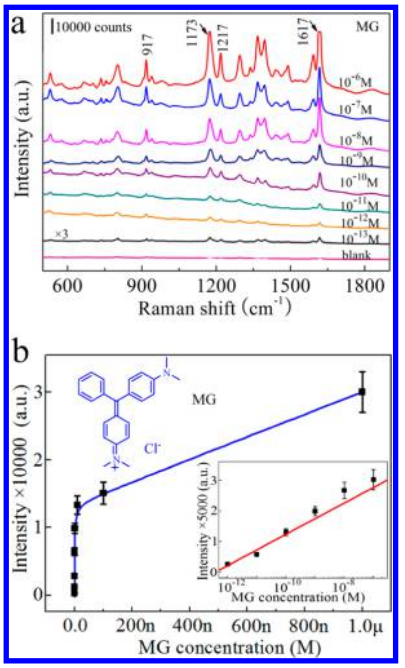

Figure 2. Results for the quantitative detection of MG, (a) concentration-dependent SERS spectra for MG detection at various concentrations (from 10^{-13} M to 10^{-6} M) on substrates, (b) plot of the peak intensity at 1173 cm^{-1} as a function of MG concentration. The inset represents the linear relationship from 10^{-12} M to 10^{-7} M.

adsorbed on substrates with various concentrations. The recorded spectra were dominated by a set of peaks located at 917, 1173, 1217, 1368, and 1617 cm^{-1}. The vibrational assignments of these peaks were summarized in Table S1 (Supporting Information). Those characteristic bands were distinguishable even at a concentration as low as 10^{-13} M. Obviously, our SERS sensing demonstrated a better sensitivity as compared to the traditional detection methods. Such sensitivity was sufficient for detection of a typical MG overdose concentration, which was generally at parts-per-million (ppm) level.

Another crucial aspect of SERS sensing for routine applications is to ensure reliable and excellent signal reproducibility. Owing to a large number of hierarchical scaffolds and AgNPs were decorated on the substrates, the SERS hotspots distributed uniformly and endowed high signal reproducibility across the whole substrate. It was investigated by collecting and superimposing the SERS signal of 30 random spots on substrates (see Figure S9a, Supporting Information). All of those Raman spectra presented clear fingerprint peaks of

DOI: 10.1021/acs.analchem.5b02788
Anal. Chem. 2015, 87, 10527−10534

MG. The intensities of peak at 1619 cm^{-1} were plotted as histogram, the mean and standard deviation was 695 ± 64.7 counts as indicated by the red dot-line (Figure S9b, Supporting Information). A statistical relative standard deviation (RSD) of these SERS intensities was 9.3% as indicated by the green shadow area. The results demonstrated a spot to spot variance of 9.3% for MG characteristic peak intensity, which was lower than the original Ag dendrites substrates (~21.3%, in Figure S10, Supporting Information), implies an excellent signal reproducibility of 3D SERS substrates.

Considering the change of nanostructure, maybe there are some main factors that contribute to the excellent reproducibility and uniformity. The first one is the great increase in the number of SERS hotspots. The hierarchical superstructure creates a 3D SERS hot-volume, which breaks the traditional limitation of 2D (or quasi-3D) substrates and extends the hotspots into the third dimension. The great improvement of the SERS hotspots (along the *z*-axis) will boost the signal uniformity of the substrates. The second one is the remarkable increase of adsorption area. The 3D superstructures offer a wide range of scaffolds, which brings about a larger overall surface area (more target molecules to be adsorbed). Finally, the hydrophilic surface enhances the affinity of the substrates significantly.

Beyond the high sensitivity and reproducibility, we further show that it is able to quantify the amount of MG present in aqueous solution. The band around 1173 cm^{-1}, which is assigned to the in-plane vibrations of ring C−H, is selected to depict the relationship between concentration and peak intensity. A plot of the dominant peak intensity against the MG concentration revealed a simple adsorption-saturation Langmuir relationship (Figure 2b). The intensities of bands increase monotonously with the concentration of MG molecule. At the low concentration range (10^{-12} to 10^{-7} M), a linear relationship between the peak intensity and the logarithm of MG concentration was observed (the inset of Figure 2b). The linear regression gave the following empirical ruler equation: I_{SERS} = 2550 log [MG] + 31687, with r = 0.97, where I_{SERS} and [MG] are the intensity of the 1173 cm^{-1} peak and concentration of the adsorbed MG, respectively. These excellent quantitative behaviors highlight the effectiveness of our 3D substrates for accurate SERS quantitative analysis of harmful substances and unapproved drugs.

In order to evaluate the selectivity of the SERS substrate toward MG, control experiments were conducted by incubating the SERS substrate in MG aqueous solution containing urea, glucose, BSA, and L-glutamine, respectively (in Figure 3a). It can be seen that exposure to some different biological organics induced a negligible response of the SERS substrate although they were the different kinds of chemical structures. As shown in Figure 3b, none of these organics caused obvious Raman signal alteration at 1617 cm^{-1}, except the amplitude and intensity of SERS signal declined slightly. Obviously, more peaks and a large background were observed in glucose, BSA, and L-glutamine contaminated MG aqueous solution (from 300 to 1500 cm^{-1}, in Figure 3a) compared with the urea contaminated MG aqueous solution and pure MG aqueous solution (without organics). This is likely due to these organics contain the organic functional groups including the $-CH_2OH$, −CHOH−, $-NH_2$, −CO−, which showed the impurities sensing. Surprisingly, we still obtained distinguishable SERS intensity of the characteristic Raman peak of MG at 1617 cm^{-1}, which does not interfere with the detection of MG and shows

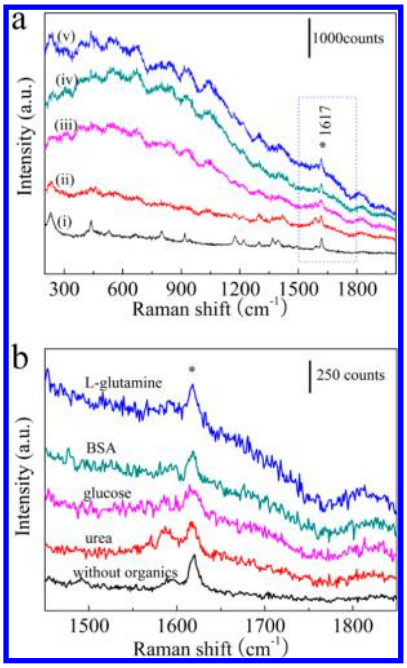

Figure 3. (a) SERS spectra of MG aqueous solutions (10^{-11} M) and the addition of L-glutamine, BSA, glucose, and urea with the concentration of 10^{-11} M (the laser power was 1.7 mW; the exposure time was 1 s). (b) The magnification of peak at 1617 cm^{-1} in part a.

excellent selectivity over other organic contaminants. Therefore, it is a convenient detection for MG without separating the organics from MG aqueous solution. Our experimental results clearly demonstrate that our SERS substrates can be used for the detection of MG from MG simulating solutions to complex environment solution.

Besides those organics, CV, a more similar chemical structures to MG, were added further for selectivity test. As shown in Figure S8a and Figure 2a, the Raman spectra of CV and MG are very close to each other, owing to their similar molecular structures. So, how to distinguish the MG molecules and estimate the content of MG (or CV) in the mixed aqueous solution remains a significant challenge. Exhilaratingly, the intensity of the characteristic bands of 1171 cm^{-1} (Figure 4a) nearly showed a progressive increase and the characteristic bands of 1219 cm^{-1} decrease with the increasing CV. Obviously, the ratio of peak intensity of 1171 over 1219 cm^{-1} was much higher in CV (bottom curve, Figure 4a) than that in MG (top curve, Figure 4a). One noticeable difference between them in Raman spectra was the ratio of peak intensity of 1171 over 1219 cm^{-1}, which were assigned to be the in-plane vibrations of ring C−H and C−H rocking, respectively.

To differentiate these two chemicals, the Raman spectra of mixed samples were tested (Figure 4a) and the value of the ratio of peak intensity of 1171 over 1219 cm^{-1} may be used to calculate the percentages of CV and MG in the mixture. Therefore, if we plot the relative Raman intensity of 1171 cm^{-1}/1219 cm^{-1} with the ratio of CV/(CV + MG) for the seven Raman spectra in Figure 4b, we may extract some quantitative information. Figure 4b shows an unbelievably linear relationship, and such linearity suggests that a quantitative relationship can be established between the relative Raman intensity and the ratio of CV. In other words, the substrates allows us to detect chemicals with similar molecular structures, such as CV, MG, and their mixture that have

DOI: 10.1021/acs.analchem.5b02788
Anal. Chem. 2015, 87, 10527−10534

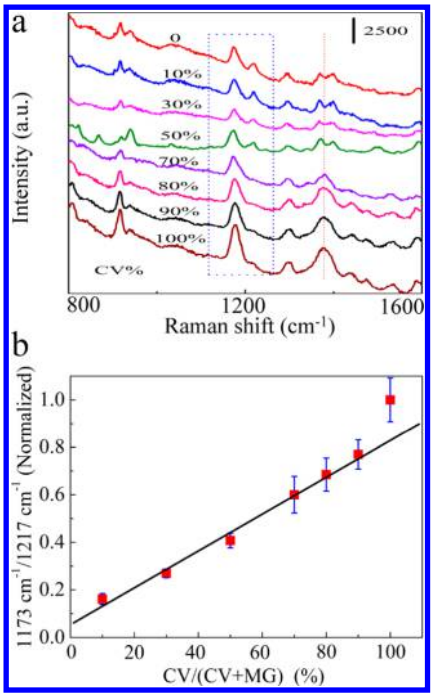

Figure 4. (a) SERS spectra of a set of mixture composed of different component of CV (the laser power was 1.7 mW; the exposure time was 5 s; the concentration of the CV (or MG) was 10^{-10} M), and in which CV% = CV/(MG + CV), (b) normalized SERS intensity at the ratio of 1173 cm^{-1}/1217 cm^{-1} versus concentration.

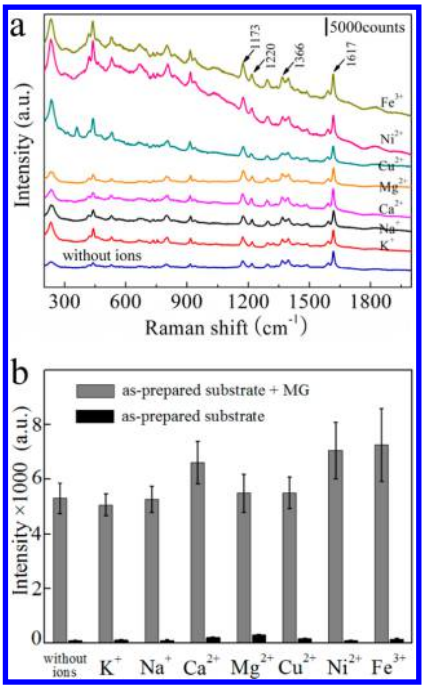

Figure 5. (a) SERS spectra of MG aqueous solutions (10^{-10} M) and the addition of K^+, Na^+, Ca^{2+}, Mg^{2+}, Cu^{2+}, Ni^{2+}, and Fe^{3+} with the concentration of 10^{-10} M (the laser power was 1.7 mW; the exposure time was 5 s). (b) The histograms of the peak at 1617 cm^{-1} which collected from part a.

different CV or MG contents, which is very important for fast screening. These results demonstrate that chemicals with similar molecular structures can be differentiated by SERS methods in conjunction with the use of our SERS substrates. Additionally, other slight differences between relative peak intensities at several positions (e.g., 916, 1380, and 1420 cm^{-1}, etc.) were also found between CV and MG. Obviously, a broad strong peak was divided into two weak peaks at 1380 cm^{-1}. These differences were likely attributed to the presence of one more CH_3-N-CH_3 in CV than in MG.

To assess the anti-interference performance, some coexistent metal ions including K^+, Na^+, Ca^{2+}, Mg^{2+}, Cu^{2+}, Ni^{2+}, and Fe^{3+} were added and examined. As shown in Figure 5a, all of Raman spectra presented clear fingerprint peaks of MG molecules such as 1173, 1220, 1336, and 1617 cm^{-1}. Obviously, none of these coexistent metal ions in solution caused obvious Raman signal shifts. Furthermore, the intensities of peaks at 1617 cm^{-1} were plotted as a histogram in Figure 5b, in order to assess the alteration of Raman intensity. After the addition of K^+, Na^+, Mg^{2+}, or Cu^{2+}, their average intensities were nearly consistent with the pure MG aqueous solutions. These coexistent metal ions have almost no influence upon the measuring accuracy and decrease the SERS signal, which verified the good selectivity of the SERS substrates. Instead, a slight enhancement was found in the addition of Ca^{2+}, Ni^{2+}, and Fe^{3+}. Importantly, the improvement of SERS intensity is conducive to the molecular recognition of SERS signal. Several possibilities may be involved in the metal ions-mediated enhancement mechanism which is being investigated by us.

Detection of MG in Spiked Environmental Water. In aquaculture, illicit drugs serving as antibacterial agent are often present in pond water. However, it is challenging to detect the trace amount of these drugs due to poor sensitivity and selectivity (small molecule drug has limited sensitivity due to the intrinsic SERS spectra at relatively low concentrations; and it exhibits poor selectivity in some complex mixtures owing to the overlapping Raman bands).

In order to verify the practicability of the proposed 3D SERS substrate, the detection of MG in spiked lake water samples was demonstrated, and the results were depicted in Figure 6. An

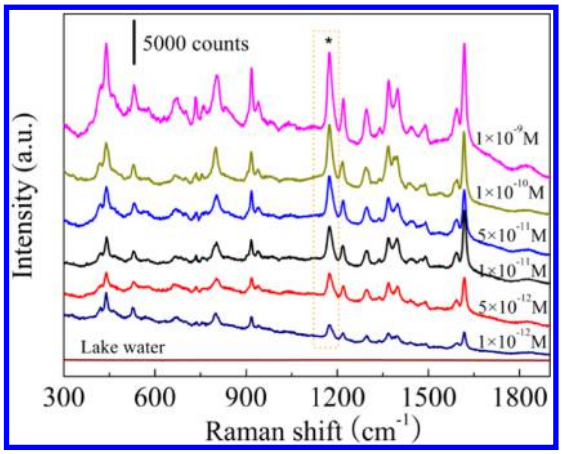

Figure 6. Detection of MG in spiked lake water.

additional purification procedure to remove the coexisting substances (such as metal ions, organics, and others) was unnecessary. The detections for MG were conducted by the incubation of the SERS substrate with the lake water which spiked with various MG concentrations. The recoveries of MG ranged from 91.2% to 109.6% with an average value of 96.9% (Table S2, Supporting Information). These results confirmed

DOI: 10.1021/acs.analchem.5b02788
Anal. Chem. 2015, 87, 10527−10534

the practical application of our 3D substrate with high accuracy and reliability.

CONCLUSION

In summary, we developed a biomimetic 3D SERS substrate with cactus-like structure for efficient and sensitive sensing. A large number of Si nanoneedle scaffolds and clusters of 20−40 nm AgNPs were successively formed on the cactus-like substrate by VLS growth and galvanic displacement, respectively, which result in concentrated SERS hotspots and high EF values as well as good reproducibility. The detection limit of MG down to 10^{-13} M was achieved. It was also able to facilely distinguish MG from some organics, coexistent metal ions, and its derivatives. Moreover, the quantification of ultratrace MG residual in environment water was successfully carried out with the recovery of 91.2% to 109.6%. Altogether, the developed cactus-like 3D SERS substrate has been proved as an efficient sensing platform with high sensitivity, reproducibility, and selectivity and may be promising in the field of sensing, imaging, and clinical diagnosis.

ASSOCIATED CONTENT

Supporting Information

The Supporting Information is available free of charge on the ACS Publications website at DOI: 10.1021/acs.analchem.5b02788.

Supplementary figures, experimental details, and the calculation process (PDF)

AUTHOR INFORMATION

Corresponding Author

*E-mail: yxzhao@mail.xjtu.edu.cn.

Author Contributions

‖J.H. and D.M. contributed equally to this work.

Notes

The authors declare no competing financial interest.

ACKNOWLEDGMENTS

The authors thank Feng Zhai for making the schemes and figures look pretty. This work was supported by Key Project of the Chinese National Programs for Fundamental Research and Development (Grant No. 2010CB631002), the National Natural Science Foundation of China (Grant Nos. 21475102 and 51171145), the Natural Science Foundation of Shanxi Province (Grant Nos. 2013JQ2017 and 2015JM5244), and the Fundamental Research Funds for the Central Universities.

REFERENCES

(1) Fleischmann, M.; Hendra, P. J.; McQuillan, A. *Chem. Phys. Lett.* **1974**, *26*, 163−166.
(2) Kurouski, D.; Van Duyne, R. P. *Anal. Chem.* **2015**, *87*, 2901−2906.
(3) Kubackova, J.; Fabriciova, G.; Miskovsky, P.; Jancura, D.; Sanchez-Cortes, S. *Anal. Chem.* **2015**, *87*, 663−669.
(4) Deng, Z.; Chen, X.; Wang, Y.; Fang, E.; Zhang, Z.; Chen, X. *Anal. Chem.* **2015**, *87*, 633−640.
(5) Guerrini, L.; Krpeti, Ž.; Lierop, D.; Alvarez-Puebla, R. A.; Graham, D. *Angew. Chem.* **2015**, *127*, 1160−1164.
(6) Lee, S.; Chon, H.; Lee, J.; Ko, J.; Chung, B. H.; Lim, D. W.; Choo, J. *Biosens. Bioelectron.* **2014**, *51*, 238−243.
(7) Zhang, Q.; Lee, Y. H.; Phang, I. Y.; Lee, C. K.; Ling, X. Y. *Small* **2014**, *10*, 2703−2711.
(8) Ho, C.-C.; Zhao, K.; Lee, T.-Y. *Nanoscale* **2014**, *6*, 8606−8611.
(9) Zhu, H.; Du, M.; Zhang, M.; Wang, P.; Bao, S.; Zou, M.; Fu, Y.; Yao, J. *Biosens. Bioelectron.* **2014**, *54*, 91−101.
(10) Gao, C.; Hu, Y.; Wang, M.; Chi, M.; Yin, Y. *J. Am. Chem. Soc.* **2014**, *136*, 7474−7479.
(11) Zeng, Y.; Pei, J.-J.; Wang, L.-H.; Shen, A.-G.; Hu, J.-M. *Biosens. Bioelectron.* **2015**, *66*, 55−61.
(12) Yang, Y.; Liu, J.; Fu, Z.-W.; Qin, D. *J. Am. Chem. Soc.* **2014**, *136*, 8153−8156.
(13) Li, J.-M.; Yang, Y.; Qin, D. *J. Mater. Chem. C* **2014**, *2*, 9934−9940.
(14) Kostovski, G.; Stoddart, P. R.; Mitchell, A. *Adv. Mater.* **2014**, *26*, 3797.
(15) Huang, Z.; Meng, G.; Huang, Q.; Yang, Y.; Zhu, C.; Tang, C. *Adv. Mater.* **2010**, *22*, 4136−4139.
(16) Liu, Y.; Zhao, L.; Su, J.; Li, M.; Guo, L. *ACS Appl. Mater. Interfaces* **2015**, *7*, 3532−3538.
(17) Cheng, C.; Yan, B.; Wong, S. M.; Li, X.; Zhou, W.; Yu, T.; Shen, Z.; Yu, H.; Fan, H. J. *ACS Appl. Mater. Interfaces* **2010**, *2*, 1824−1828.
(18) Tan, Y.; Gu, J.; Xu, L.; Zang, X.; Liu, D.; Zhang, W.; Liu, Q.; Zhu, S.; Su, H.; Feng, C. *Adv. Funct. Mater.* **2012**, *22*, 1578−1585.
(19) Tan, Y.; Gu, J.; Xu, W.; Chen, Z.; Liu, D.; Liu, Q.; Zhang, D. *ACS Appl. Mater. Interfaces* **2013**, *5*, 9878−9882.
(20) Wang, L.; Li, H.; Tian, J.; Sun, X. *ACS Appl. Mater. Interfaces* **2010**, *2*, 2987−2991.
(21) Ye, W.; Chen, Y.; Zhou, F.; Wang, C.; Li, Y. *J. Mater. Chem.* **2012**, *22*, 18327−18334.
(22) Ren, W.; Guo, S.; Dong, S.; Wang, E. *Nanoscale* **2011**, *3*, 2241−2246.
(23) Ho, J.-Y.; Liu, T.-Y; Wei, J.-C.; Wang, J.-K.; Wang, Y.-L.; Lin, J.-J. *ACS Appl. Mater. Interfaces* **2014**, *6*, 1541−1549.
(24) Liu, X.; Zong, C.; Ai, K.; He, W.; Lu, L. *ACS Appl. Mater. Interfaces* **2012**, *4*, 6599−6608.
(25) Cao, M.; Ju, J.; Li, K.; Dou, S.; Liu, K.; Jiang, L. *Adv. Funct. Mater.* **2014**, *24*, 3235−3240.
(26) Heng, X.; Xiang, M.; Lu, Z.; Luo, C. *ACS Appl. Mater. Interfaces* **2014**, *6*, 8032−8041.
(27) Peng, F.; Su, Y.; Zhong, Y.; Fan, C.; Lee, S.-T.; He, Y. *Acc. Chem. Res.* **2014**, *47*, 612−623.
(28) McLellan, J. M.; Siekkinen, A.; Chen, J.; Xia, Y. *Chem. Phys. Lett.* **2006**, *427*, 122−126.
(29) Huang, J.; Chen, F.; Zhang, Q.; Zhan, Y.; Ma, D.; Xu, K.; Zhao, Y. *ACS Appl. Mater. Interfaces* **2015**, *7*, 5725−5735.
(30) Reuben, D.; Bruice, T. C. *J. Am. Chem. Soc.* **1976**, *98*, 114−121.
(31) Qian, Y.; Meng, G.; Huang, Q.; Zhu, C.; Huang, Z.; Sun, K.; Chen, B. *Nanoscale* **2014**, *6*, 4781−4788.
(32) Shao, F.; Lu, Z.; Liu, C.; Han, H.; Chen, K.; Li, W.; He, Q.; Peng, H.; Chen, J. *ACS Appl. Mater. Interfaces* **2014**, *6*, 6281−6289.
(33) Yan, M.; Xiang, Y.; Liu, L.; Chai, L.; Li, X.; Feng, T. *RSC Adv.* **2014**, *4*, 98−104.
(34) Hannon, J.; Kodambaka, S.; Ross, F.; Tromp, R. *Nature* **2006**, *440*, 69−71.
(35) Sivasubramanian, R.; Sangaranarayanan, M. *Sens. Actuators, B* **2015**, *213*, 92−101.
(36) Le Ru, E.; Blackie, E.; Meyer, M.; Etchegoin, P. G. *J. Phys. Chem. C* **2007**, *111*, 13794−13803.
(37) Bordon, Y. *Nat. Rev. Immunol.* **2015**, *15*, 200−201.
(38) Abbott, A. *Nature* **2014**, *513*, 290−290.
(39) Dong, J.-X.; Xu, C.; Wang, H.; Xiao, Z.-L.; Gee, S. J.; Li, Z.-F.; Wang, F.; Wu, W.-J.; Shen, Y.-D.; Yang, J.-Y. *J. Agric. Food Chem.* **2014**, *62*, 8752−8758.
(40) Ahmad, A.; Mohd-Setapar, S. H.; Chuong, C. S.; Khatoon, A.; Wani, W. A.; Kumar, R.; Rafatullah, M. *RSC Adv.* **2015**, *5*, 30801−30818.
(41) Yin, R.; Mo, J.; Lu, M.; Wang, H. *Anal. Chem.* **2015**, *87*, 1846−1852.
(42) Lanucara, F.; Holman, S. W.; Gray, C. J.; Eyers, C. E. *Nat. Chem.* **2014**, *6*, 281−294.
(43) Hao, Y.; Guo, Q.; Wu, H.; Guo, L.; Zhong, L.; Wang, J.; Lin, T.; Fu, F.; Chen, G. *Biosens. Bioelectron.* **2014**, *52*, 261−264.

DOI: 10.1021/acs.analchem.5b02788
Anal. Chem. 2015, 87, 10527−10534

(44) Dutta, S.; Ray, C.; Mallick, S.; Sarkar, S.; Roy, A.; Pal, T. *RSC Adv.* **2015**, *5*, 51690−51700.
(45) Lang, Q.; Wang, F.; Yin, L.; Liu, M.; Petrenko, V. A.; Liu, A. *Anal. Chem.* **2014**, *86*, 2767−2774.
(46) Aroonyadet, N.; Wang, X.; Song, Y.; Chen, H.; Cote, R. J.; Thompson, M. E.; Datar, R. H.; Zhou, C. *Nano Lett.* **2015**, *15*, 1943−1951.

DOI: 10.1021/acs.analchem.5b02788
Anal. Chem. 2015, 87, 10527−10534